Separation and Purification Technology 116 (2013) 458–470

Contents lists available at SciVerse ScienceDirect

Separation and Purification Technology

journal homepage: www.elsevier.com/locate/seppur

Reliable prediction of condensation rates for purification of natural gas via supersonic separators

S.H. Rajaee Shooshtari, A. Shahsavand *

Department of Chemical Engineering, Faculty of Engineering, Ferdowsi University of Mashhad, Mashhad, Iran

ARTICLE INFO

Article history:
Received 2 March 2013
Accepted 8 June 2013
Available online 13 June 2013

Keywords:
Supersonic separator
Droplet growth
Natural gas
Dehumidification
Sweetening

ABSTRACT

Supersonic separators can provide efficient and simultaneous separation and purification of natural gases from various impurities (e.g. water vapor and hydrogen sulfide). Reliable prediction of the liquid droplet growth inside Laval nozzle is essential for accurate simulation of the condensation process inside 3S unit. All previous researches have been focused on estimation of the liquid droplet growth for pure fluids (e.g. steam) and cannot be extended to binary or multi-component systems. The current article provides a new theoretical approach based on mass transfer rate calculations to predict the liquid droplet growth inside a Laval nozzle for binary mixtures. The current model can be also used to simulate the multi-component systems when no appreciable interaction exists between the condensed phases. The new model predictions are initially validated successfully with the experimental data borrowed from the literature. Afterwards, several natural gas processes are simulated inside Laval nozzles of various 3S units. The simulation results indicate that the 3S unit is able to successfully reduce both water vapor and hydrogen sulfide content of natural gas to their permissible values (7lb/MMSCF and 4 ppm, respectively) for all cases.

1. Introduction

Supersonic separators (3S) provide numerous applications in oil and gas industries such as Gas conditioning (dehydration and dehumidification of natural gas), extraction of heavy hydrocarbons from methane (Ethane or Liquefied Petroleum Gases (LPG) recovery), separation of carbon dioxide and hydrogen sulfide from natural gases and production of Liquefied Natural Gas (LNG). Solvent processing, use of membranes, adsorption and cryogenic separations can be used for separation and purification of natural gas from various impurities [1–4]. These technologies require relatively large facilities, high capital and operating investment and many operational problems. Supersonic separators are well suited for those tasks, because they create extremely low temperatures inside Laval nozzle which can easily lead to condensations of almost all impurities from methane. For this reason, they provide a new and powerful choice for dehydration and sweetening of almost any natural gas.

Fig. 1 shows that Laval nozzles play a critical role in the structure of Super Sonic Separators (3S units), especially before collection point. 3S units combine adiabatic cooling and cyclonic separation in a single compact device. The gas enters the swirling section of 3S (plenum chamber) with a relatively low velocity and high pressure at operating temperature. A set of static vanes are positioned in the plenum chamber to induce massive swirling motion inside process fluid. The gas velocity increases to extremely high values (Ma > 1) when it passes through the nozzle-diffuser segments of the Laval nozzle. Evidently, the fluid pressure erratically reduces due to the transformation of potential energy into kinetic energy [5].

As a result of adiabatic expansion, the gas temperature drops quickly and all condensable species (e.g. water or heavy hydrocarbons) condense in extremely cooled supersonic section of the Laval nozzle. Gigantic centrifugal accelerations (300,000–500,000 g) are anticipated due to the combination of supersonic flow of the gas stream and strong swirling motion induced by the plenum chamber. Under such extreme centrifugal forces, the liquid droplets are thrown away towards the diffuser wall, leaving the 3S by a circumferential passage at collection point. The relatively liquid-free gas stream passes the separation point with extremely low temperature and pressure (near-100 °C and one fourth of inlet pressure), while still retaining its very high velocity (Ma > 1). Since higher operating pressure and temperature are desired for proper transmission of natural gas after separation, therefore the fluid should be decelerated after collection point for pressure recovery purposes. This task can be achieved by using various scenarios such as normal shock wave occurrence or recruiting a second Laval nozzle as described in our previous works [6].

* Corresponding author. Tel.: +98 915 514 9544; fax: +98 511 8816840.
E-mail address: shahsavand@um.ac.ir (A. Shahsavand).

1383-5866/$ - see front matter © 2013 Elsevier B.V. All rights reserved.
http://dx.doi.org/10.1016/j.seppur.2013.06.009

Nomenclature

A	area
a	speed of sound
B_1	second virial coefficient
C	concentration
C_p	specific heat at constant pressure
D	diffusion coefficient
d_e	hydraulic diameter
f	friction factor
h	enthalpy
h_{fg}	latent heat
J	rate of formation of droplets per unit volume and time
J_A	diffusion rate of species A
k	Boltzmann constant(1.3807×10^{-23} J/K)
m	mass of single molecule
m_d	mass of single droplet
$\dot{m}$	mass flow rate
M	molecular weight
Ma	mach number
N	Avogadro's number (6.02×10^{23} molecules/mole)
N_β	mass transfer rate of species β
P	pressure
$P^{sat}(T_L)$	saturation pressure at T_L
q_c	condensation coefficient
r	radius
R	gas constant
$\hat{R}$	gas constant on a mass basis
R_d	mean droplet radius
S	super-saturation ratio
T	temperature
T_L	droplet temperature
U	velocity
V^l	liquid specific volume
V^g	gas specific volume
V_{segj}	volume of segment j
WEtOH	mass fraction of ethanol
Z	square of mach number
z	compressibility factor
γ	specific heat capacity ratio
ρ	density
σ	surface tension
η	non-isothermal correction factor

Subscripts

b	bulk
G	vapor phase
L	liquid phase
in	inlet
t	total
α	non-condensable gas
β	condensable gas

Superscripts

$*$	critical
sat	saturation

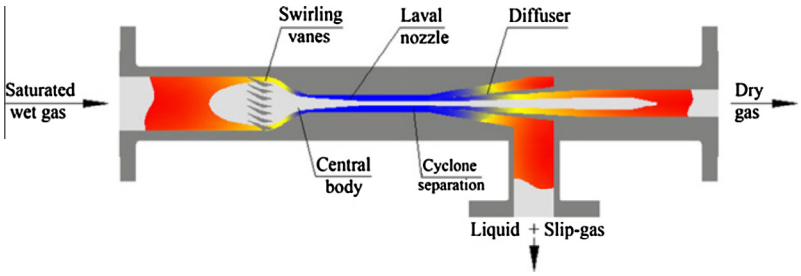

Fig. 1. Schematic diagram of a supersonic separator.

Supersonic separators are traditionally used for dehumidification of natural gases [7]. The wet gas enters the Laval nozzle at saturated condition and expands to sonic condition at the throat location. Evidently, gas pressure and temperature are drastically reduced due to the sudden increase in the gas velocity. When super-saturation ratio is greater than unity, droplet embryos begin to form and grow inside Laval nozzle [8]. The pressure reduction continues more intensely due to the nucleation rates associated with these early embryos and the corresponding droplet growth for previously formed droplets. After this point, nucleation ceases effectively and the number of droplets in the flow remains nearly constant [8]. In this region, the droplets grow rapidly and cause a sudden jump in pressure profile due to the release of latent heat at supersonic conditions which tends to retard the supersonic flow. This point is usually referred to as Wilson point.

After nucleation, the mole fraction of water vapor inside the natural gas stream begins to reduce until dehumidification process will be complete. The condensed liquid should be separated from the gas stream otherwise the liquid vaporizes again upon pressure recovery. The entire process takes less than 2 ms [9].

Twister BV (Netherlands) engineers presented various applications of supersonic separators including natural gas dehydration, hydrocarbon dew point control, deep liquid recovery and hydrogen sulfide removal during 2002–2008 [7,10–12]. In 2003, Alferov et al. [13] and Betting et al. [14] proposed a method and apparatus for the separation and liquefaction of the gas mixtures. Liu et al. [15] described a natural gas dehydration unit and presented the corresponding structure and its working principles. The test results for an indoor 3S rig revealed that the pressure loss ratio, the shock wave location and the fluid flow rate had immense effect on the overall dehydration characteristics of the entire process.

Jassim et al. [16,17] studied the flow behavior of high-pressure natural gas in supersonic nozzles by CFD technique. The effects of real gas, nozzle geometry and the vorticity on the performance of Laval nozzle were also investigated. They reported that shock wave position can significantly change when the gas is considered as real

rather than perfect and although losses in pressure increase due to inlet swirl flow, but vorticity increases very sharply in the vicinity of the shock. Malyshkina [18] presented a two-dimensional Euler model for analysis of gas-dynamic parameters under conditions of separation in the region of shock wave and behind it. Karimi and Abdi [19] presented a selective dehydration of high-pressure natural gas using supersonic nozzles. The influences of the inlet pressure, temperature and back pressure on the shock positions were discussed. Their results showed that by increasing the inlet back pressure and decreasing the inlet temperature, the normal shock wave occurs earlier.

In 2010, Malyshkina [20] studied the supersonic separator performance for high temperature separation of natural gas into its components. The compositions of gas–liquid mixtures were determined as a function of initial parameters. In 2011 and 2012 Wen et al. [21–23] investigated the effects of the supersonic swirling flow on the radial distribution of the main parameters of gas flow inside 3S unit. They also studied the effect of shock wave position and the particle trajectories and separation efficiency by using the Discrete Particle Method (DPM).

Ghanbari Mazidi et al. [6] examined the performances of two supersonic separator structures when pressure recovery accomplished via a normal shock wave or two consecutive nozzle-diffusers are used. They reported that the first structure provides more flexibility but may fail drastically if the normal shock wave location precedes the liquid collection point.

The above articles investigated the 3S unit performances in the absence of nucleation and growth phenomena. The following researches focused on these issues.

Gyarmathy [24] predicted the growth rate of water droplets from condensing steam over a wide range of pressure and flow regimes from free molecule to continuum. Young [25] introduced the droplet growth parameters α, which presented a relationship between evaporation and condensation coefficients. Bakhtar and Zidi [26] presented a semi-empirical relation for droplet's growth. Gyarmathy [27] provided a fairly realistic approximation for temperature of submicron droplets by considering the capillarity effect and assuming uniform droplet temperature inside droplets.

Koo et al. [28] presented a one-dimensional model based on classical nucleation and growth as a diagnostic tool for predicting the impact of different process conditions and nozzle geometries on particle size distributions produced from supersonic quenching of magnesium vapors. Among many others, Bakhtart and Mohammadi Tochai [29], Guha and Young [30], Cinar et al. [31], White and Hounslow [32], Dykas [33], Gerber and Kermani [34], Mahpeykar and Teymourtash [35], Yang and Shen [36] and Dykas and Wroblewski [37] used essentially a similar procedure for estimation of various operating conditions and the corresponding mean droplets radius during the flow of supersonic gas inside Laval nozzle [29–37]. All of these researches focused on pure component system.

As mentioned above, several simulations of Laval nozzles have been previously reported in the literature. A new model is presented in this article to model the self-condensation phenomenon in nozzle-diffusers for binary system. The proposed model extends the traditional nucleation and growth process for binary systems [37]. Multi-component mass transfer approach (which was originally presented in our previous work [38]) will be used instead of single component empirical correlations to compute the droplet growth along the nozzle. To the best our knowledge, the present method has not been addressed previously.

2. Mathematical model for binary systems

Assuming no inter-phase slippage and steady state flow condition, the one dimensional governing equations for two-phase flow of a condensable stream over any segment of an incremental distance dx inside a converging–diverging nozzle can be written as:

2.1. Continuity

Assuming negligible area occupied by liquid droplets, continuity equation in each section becomes:

$$\dot{m}_t = \dot{m}_L + \dot{m}_\alpha + \dot{m}_\beta \tag{1}$$

where $\dot{m}$ denotes the mass flow rate and the subscripts t, L, α and β indicate total, liquid, non-condensable gas (e.g. methane) and condensable vapor (e.g. steam or H_2S), respectively. Defining $\dot{m}_G$ as the summation of non-condensable and condensable mass flow rates:

$$\dot{m}_G = \dot{m}_\alpha + \dot{m}_\beta = \rho_G A U_G \tag{2}$$

where ρ_G is the gas phase density at operating condition (computable from any proper equation of state using appropriate mixing rule), A is the total cross-sectional area of nozzle at any segment and U_G is the corresponding gas velocity. Differentiating Eq. (1) leads to:

$$\frac{d\rho_G}{\rho_G} + \frac{dA}{A} + \frac{dU_G}{U_G} + \frac{d\dot{m}_L}{\dot{m}_t - \dot{m}_L} = 0 \tag{3}$$

2.2. Momentum equation

The one dimensional momentum changes across element dx can be expressed as:

$$d[\dot{m}_G U_G + \dot{m}_L U_L] = -A dP - \frac{f A \rho_G U_G^2}{2 d_e} dx \tag{4}$$

where f is the Fanning friction factor and d_e is the hydraulic diameter. Assuming no slippage between the gas and liquid phases ($U_G = U_L$) and dividing Eq. (4) by ($A \times P$), the momentum equation can be simplified and rearranged as:

$$\frac{dP}{P} = -\frac{f \rho_G U_G^2}{2P}\frac{dx}{d_e} - \frac{m_t U_G}{AP}\frac{dU_G}{U_G} \tag{5}$$

2.3. Equation of state

Using first order Virial equation of state (EOS), the compressibility factor for the gas stream at any location can be computed from:

$$z = \frac{P}{\rho_G \hat{R} T_G} = 1 + B_1 \rho_G \tag{6}$$

where $\hat{R}$ is the universal gas constant on a mass basis and second viral coefficient (B_1) depends on the process temperature. On differentiation, Eq. (6) becomes:

$$\begin{gathered} \frac{dP}{P} - X\frac{d\rho_G}{\rho_G} - Y\frac{dT_G}{T_G} = 0 \\ X = \frac{\rho_G}{P}\left(\frac{\partial P}{\partial \rho_G}\right)_{T_G} = \frac{1+2B_1\rho_G}{1+B_1\rho_G} \\ Y = \frac{T_G}{P}\left(\frac{\partial P}{\partial T_G}\right)_{\rho_G} = 1 + \frac{\rho_G T_G}{1+B_1\rho_G}\left(\frac{dB_1}{dT_G}\right) \end{gathered} \tag{7}$$

2.4. Energy equation

The energy equation for steady state adiabatic flow at any section can be written as:

$$d\left[\dot{m}_G\left(h_G + \frac{U_G^2}{2}\right) + \dot{m}_L\left(h_L + \frac{U_L^2}{2}\right)\right] = 0 \tag{8}$$

where h_G and h_L are the gas and liquid enthalpies, respectively. The change of enthalpy of the vapor phase can be expressed by:

$$dh_G = \left(\frac{\partial h_G}{\partial T_G}\right)_P dT_G + \left(\frac{\partial h_G}{\partial P}\right)_{T_G} dP = c_P dT_G + \left[V_G - T_G\left(\frac{\partial V_G}{\partial T_G}\right)_P\right] dP \quad (9)$$

Dividing Eq. (8) by $\dot{m}_t c_p T_G$ and replacing latent heat $(h_G - h_L)$ with h_{fg}, then using Eq. (2) for $\dot{m}_G$ and equation of state for V_G and $\left(\frac{\partial V_G}{\partial T_G}\right)_P$ leads to the following equation which usually provides the gas temperature at each segment.

$$\frac{dT_G}{T_G} + \frac{P}{\rho_G c_p T_G}\left(1 - \frac{Y}{X}\right)\frac{dP}{P} + \frac{U_G}{c_p T_G}\frac{dU_G}{U_G} - \frac{h_{fg}}{C_p T_G}\frac{d\dot{m}_L}{\dot{m}_t} = 0 \quad (10)$$

2.5. Mach number

Assuming small condensation rates, the speed of sound in a single phase fluid gas can be expressed as:

$$a = \sqrt{\frac{\gamma P}{\rho_G}} \quad (11)$$

where γ is the ratio of specific heats. Introducing Z as the square of Mach number value:

$$Z = Ma^2 = \frac{U_G^2 \rho_G}{\gamma P} \quad (12)$$

Differentiating the above equation and rearranging it leads to:

$$\frac{dZ}{Z} = 2\frac{dU_G}{U_G} + \frac{d\rho_G}{\rho_G} - \frac{dP}{P} \quad (13)$$

2.6. Liquid mass flow rate

Liquid mass flow rate at each increment can be calculated by computing the nucleation and growth rates for a binary system.

2.6.1. Nucleation rate

Assuming that the initial liquid embryos form only at a critical radius (r^*), then the nucleation rate (J) can be computed by resorting to the definition of Dirac-delta function [39]:

$$J(r^*) = \int J^*(r)\delta(r - r^*)dr = J^*(r^*) \quad (14)$$

The critical radius (r^*) is given via Kelvin–Helmholtz equation [40]:

$$r^* = \frac{2\sigma_\beta}{\rho_L R T_G \ln S_\beta} \approx \frac{2\sigma_\beta T^{sat}(P_\beta)}{\rho_L h_{fg}(T_G - T^{sat}(P_\beta))} \quad (15)$$

where σ_β and S_β are the surface tension and super-saturation ratio of the condensable specie β. The rate of nucleation can be calculated from the classical nucleation theory and modified to include non-isothermal effects as [40,41]:

$$J^* = \frac{q_c}{1+\eta}\frac{\rho_\beta^2}{\rho_L}\sqrt{\frac{2\sigma_\beta}{\pi m_\beta}}\exp\left(-\frac{4\pi r^{*2}\sigma_\beta}{3kT_G}\right) \quad (16)$$

where q_c is the condensation coefficient and has a value between 0.02 and 1.5 and can be calculated from following correlation: [42]

$$q_c = \left(1 - \sqrt[3]{\frac{V^l}{V^g}}\right)\exp\left(-\frac{1}{2}\frac{1}{\sqrt[3]{\frac{V^g}{V^l} - 1}}\right)$$

In the above equations, the parameters V^l and V^g are the gas and liquid specific volumes, respectively while m_β and k are the mass of a single molecule of condensable component (β) and the Boltzmann constant (1.3807×10^{-23} J/K). The non-isothermal correction factor η is defined as:

$$\eta = \frac{2(\gamma - 1)}{1 + \gamma}\frac{h_{fg}}{RT_G}\left(\frac{h_{fg}}{RT_G} - 0.5\right) \quad (17)$$

2.6.2. Growth rate

Traditional correlations for calculating the growth rate in a self-condensation process cannot be used for binary or multi-component system.

A novel procedure based on mass transfer approach is presented in this section for calculation of growth rate of multi-component systems. In this approach, mass balance over a single droplet during growth process inside a Laval nozzle can be written as:

$$\frac{dm_d}{dt} = N_\beta M_\beta A \quad (18)$$

where m_d is the mass of single droplet $(m_d = (4/3)\rho_L \pi R_d^3)$ and N_β is the molar flux of condensation rate for condensable specie β (such as water vapor).

To compute the mass transfer rate (N_β) for Eq. (18), mole balance on a spherical shell of thickness Δr outside of a single droplet for species β becomes:

accumulation = in − out + generation − consumption

$$\frac{d}{dt}(4\pi r^2 \Delta r C_\beta) = (N_\beta 4\pi r^2)|_{r+\Delta r} - (N_\beta 4\pi r^2)|_r + 0 - 0 \quad (19)$$

Rearrangement of above equation by resorting to the definition of simple differentiation, leads to:

$$r^2\frac{dC_\beta}{dt} = \lim_{\Delta r \to 0}\frac{(N_\beta r^2)|_{r+\Delta r} - (N_\beta r^2)|_r}{\Delta r} = \frac{\partial}{\partial r}(r^2 N_\beta) \quad (20)$$

Total mass transfer rate is comprised of bulk flow and binary diffusion as:

$$N_\beta = N_{\beta b} + J_\beta = N_{\beta b} - D_{\beta\alpha}\frac{dC_\beta}{dr} \quad (21)$$

where $D_{\beta\alpha}$ is the binary diffusion coefficient. The convective term in Eq. (21) (i.e.$N_{\beta b}$) can be neglected due to the no inter-phase slip assumption. Substituting for N_β from Eq. (21) into right hand side of Eq. (20) leads to:

$$r^2\frac{\partial C_\beta}{\partial t} = -D_{\beta\alpha}\left(r^2\frac{\partial^2 C_\beta}{\partial r^2} + 2r\frac{\partial C_\beta}{\partial r}\right) \quad (22)$$

Since r never becomes zero during the growth process, then the above equation reduces to:

$$\frac{\partial C_\beta}{\partial t} = -D_{\beta\alpha}\left(\frac{\partial^2 C_\beta}{\partial r^2} + \frac{2}{r}\frac{\partial C_\beta}{\partial r}\right) \quad (23)$$

The above partial differential equation should be solved with the following initial and boundary conditions:

I.C : at $t = 0$ and any r $C_\beta = C_{\beta b}$

B.C.1 : at $r = R_d$ and any t $C_\beta = C_\beta^{sat}$

B.C.1 : at $r \to \infty$ and any t $C_\beta = C_{\beta b}$

where C_β^{sat} and $C_{\beta b}$ are the concentrations of the condensable species β at the surface of the droplet and in the bulk of gas stream. Both of these concentrations can be defined as:

$$C_\beta^{sat} = \frac{P^{sat}(T_L)}{z(T_L, P^{sat})RT_L} \quad (24)$$

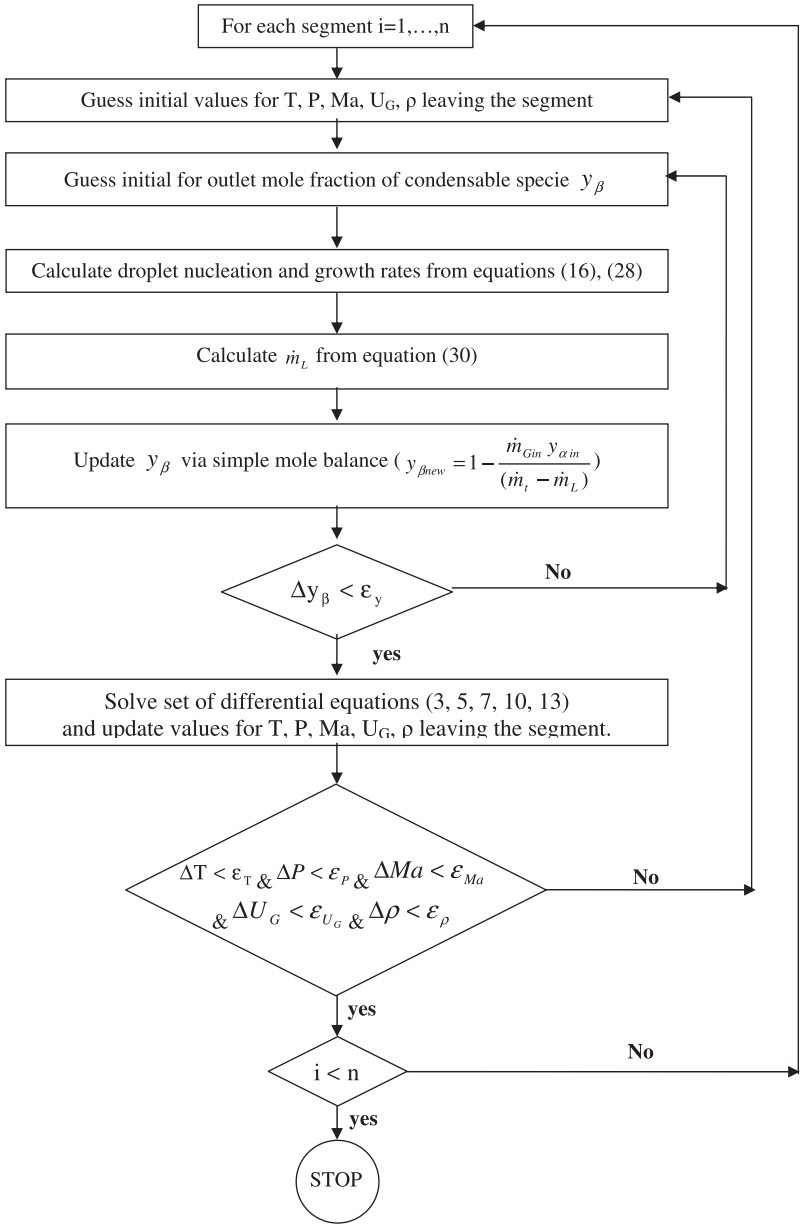

Fig. 2. Computation algorithm for calculation of operating parameters across each segment.

$$C_{\beta b} = \frac{P y_\beta}{z\,(T_G, P)\, R T_G} \tag{25}$$

Eq. (23) can be solved via Laplace transform which provides the following solution:

$$\frac{C_\beta - C_{\beta b}}{C_\beta^{sat} - C_{\beta b}} = -\frac{R_d}{r}\, erfc\left(\frac{(r - R_d)}{2\sqrt{D_{\beta\alpha} t}}\right) \tag{26}$$

Substituting C_β in simplified version of Eq. (21), the condensation (mass transfer) rate over a spherical droplet can be obtained as:

$$N_B = -D_{\beta\alpha}\frac{dC_\beta}{dr}|_{r=R_d} = D_{\beta\alpha}\left(C_{\beta b} - C_\beta^{sat}\right)\frac{\sqrt{\pi D_{\beta\alpha} t} + R_d}{R_d\sqrt{\pi D_{\beta\alpha} t}} \tag{27}$$

Replacing N_β from above equation into Eq. (18) results:

$$\frac{dR_d}{dt} = \frac{D_{\beta\alpha} M_\beta \frac{\sqrt{\pi D_{\beta\alpha} t} + R_d}{R_d\sqrt{\pi D_{\beta\alpha} t}}}{\rho_L}\left(\frac{P y_\beta}{z\,(T_G, P)\, R T_G} - \frac{P^{sat}(T_L)}{z(T_L, P^{sat})\, R T_L}\right) \tag{28}$$

Table 1
Nozzle geometry and stagnation conditions used in experimental data [43].

Prameter	Unit	Value
Throat radius	m	0.006373
Exit radius	m	0.01136
Length of diverging section	m	0.057
Stagnation pressure	Kpa	83.4
Stagnation temprature	K	296

Neglecting the temperature difference between the gas stream inside Laval nozzle and the growing droplets ($T_G = T_L$), then Eq. (28) can provide the droplet growth rate when coupled with the previous Eqs. (1)–(17). Finally, liquid mass generation rate at each segment (j) should be calculated from the following relation:

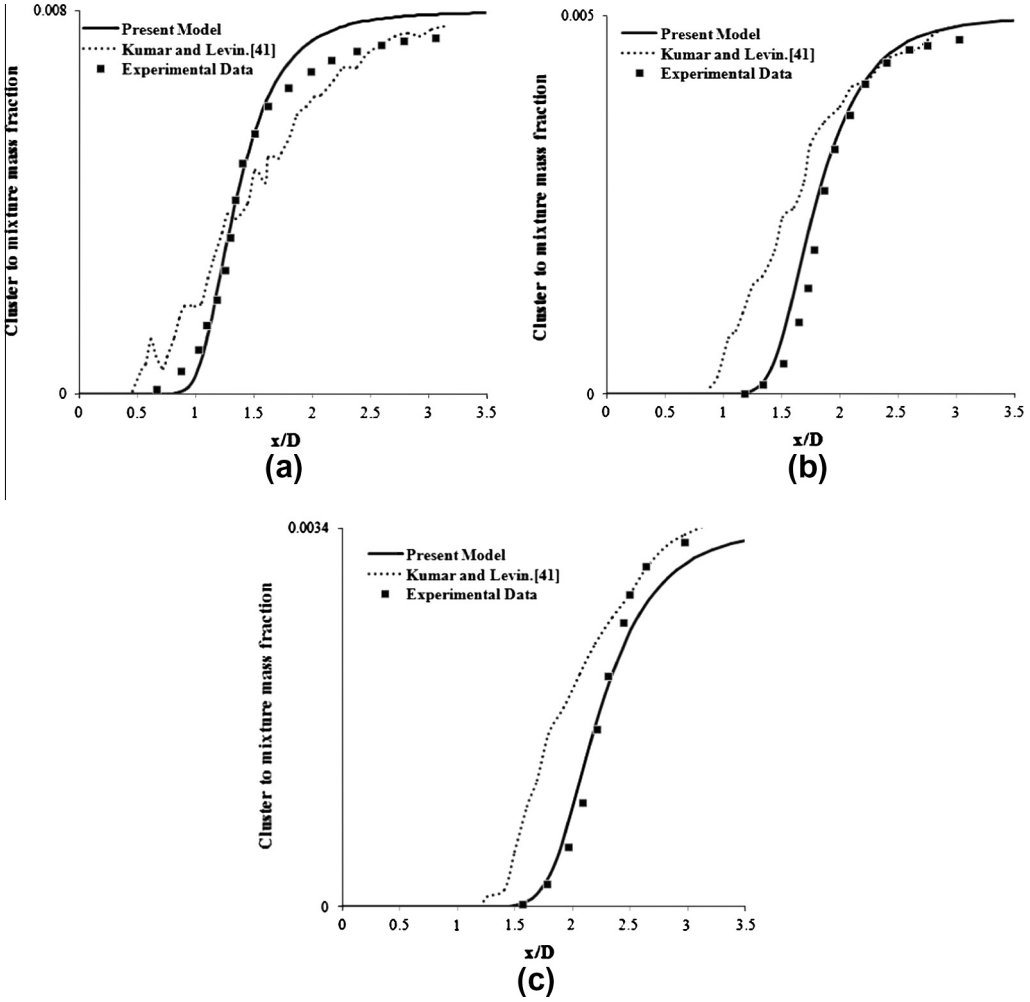

Fig. 3. Comparison of simulation results with experimental data of Wegener et al. [43] for cluster to mixture fraction (a) WEtOH = 0.008 (b) WEtOH = 0.005 and (c) WEtOH = 0.0034.

$$\dot{m}_{Lsegj} = \left(4/3\,\pi r_j^{*3}\rho_L J_j V_{segj}\right) + \left(4/3\,\pi\rho_L\left(\sum_{i=1}^{j-1} J_i V_{segi}\right)\left((R_d+dr)^3 - R_d^3\right)\right) \quad (29)$$

Ultimately, the total liquid mass flow rate at any segment (j) is given by the following equation:

$$\dot{m}_L = \sum_{i=1}^{j} \dot{m}_{Lsegi} \quad (30)$$

Fig. 2 shows the computation algorithm for calculation of all unknown variables (pressure, temperature, velocity, density, liquid mass flow rate, nucleation rate and droplet radius) at each segment of the 3S unit before collection point for binary systems.In contrast to the traditional modeling available in the literature, the above formulation is not limited to the pure component systems and can be used for separation of any condensable gas (vapor) from any desired non-condensable stream.

3. Model validation

The experimental data of Wegener et al. [43] for condensation of ethanol vapor from air stream in Laval nozzle are borrowed from literature [44] to validate our newly proposed model for binary systems. The experiments were conducted at three different ethanol mass fraction (0.0034, 0.005, 0.008) in the air stream entering the Laval nozzle. Table 1 provides the nozzle geometry and the stagnation (boundary) condition used in the experiments.

3.1. Validation test results

The novel formulation described in the previous section is used along with the stagnation conditions reported by Wegener et al. [43] to simulate the ethanol droplets growth rate inside the Laval nozzle of the 3S unit. Figs. 3–7 compares our simulation results with the recent work of Kumar and Levin [44]. They used the Bhatnagar-Gross-Krookbsd approach coupled with the following equation for prediction of droplet growth:

$$C = \frac{4\pi R_d^2 q P}{\sqrt{2\pi m k T}} \quad (31)$$

In their model, m is the molecular mass and q is the cluster-monomer sticking probability [44]. In the original article of Wegener et al., the cluster term represents the condensed phase or the entire cloud of liquid droplets.Figs. 3 and 4 compares the impressive simulations results of our present theoretical model and predictions of Kumar and Levin with the experimental data reported by Wegener

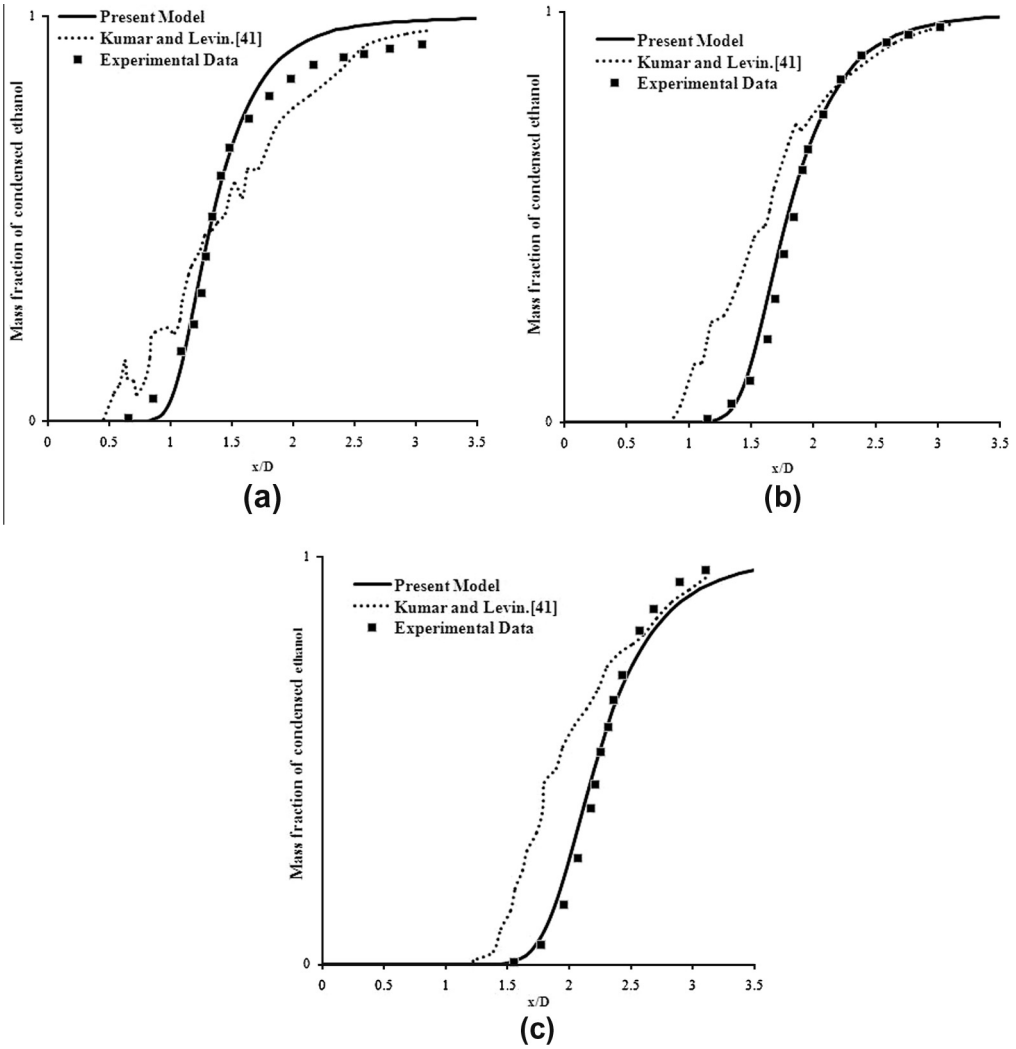

Fig. 4. Comparison of simulation results with experimental data of Wegener et al. [43] for mass fraction of condensed ethanol (a) WEtOH = 0.008 (b) WEtOH = 0.005 and (c) WEtOH = 0.0034.

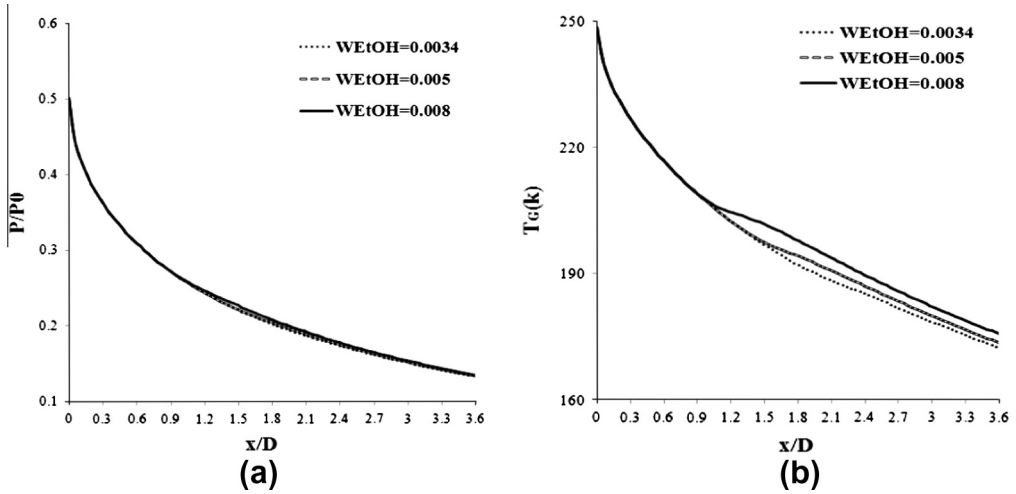

Fig. 5. Simulation results for distribution of operating conditions across Laval nozzle. (a) pressure ratio and (b) temperature.

et al. for variations of cluster to mixture fraction and mass fraction of condensed ethanol with dimensionless length[1] (x/D) for various ethanol vapor mass fraction at 3S entrance (throat). As it can be seen, our model is strongly validated and the present approach can be used as a powerful and accurate tool for design and analysis of Laval nozzle behavior in supersonic separator for binary systems.

[1] D: Throat diameter.

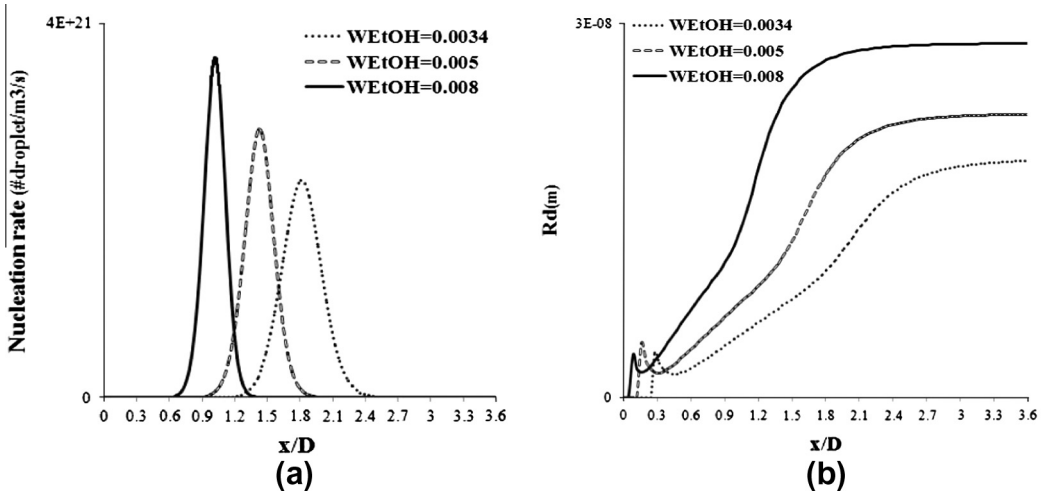

Fig. 6. Simulation results for distribution of nucleation rate (a) and condensed ethanol droplet radius (b).

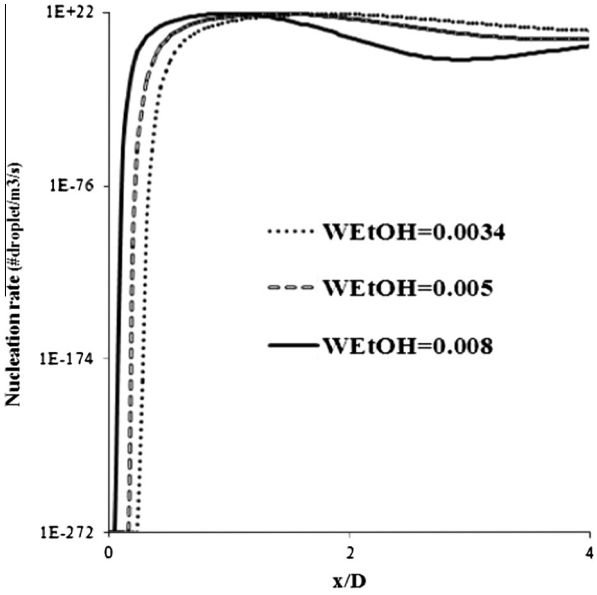

Fig. 7. Simulation results for distribution of nucleation rate in semi-log scale.

Table 2
Nozzle parameters.

Parameter	Unit	Value
Inlet radius	m	0.0513
Inlet area	m^2	0.0083
Throat radius	m	0.05
Throat area	m^2	0.0079
Outlet radius	m	0.094
Outlet area	m^2	0.0278
Nozzle (converging) length	m	0.1
Diffuser (diverging) length	m	1

Fig. 5 illustrates the corresponding simulation results for the temperature and pressure profiles across the diverging section of the Laval nozzle for various ethanol vapor mass fractions at 3S entrance (throat). As it can be seen, different ethanol vapor mass fractions do not affect the pressure distribution. Because, all vapor mass fractions are very small and essentially negligible when compared to air mass fractions at the throat conditions. In a similar manner, the temperature profiles are initially the same for

Table 3
Analysis and operating conditions of wet feed gas entering dehumidification process.

Parameter	Unit	Value
CH_4 composition	Mole Fraction	0.9991099
Water vapor (saturated at inlet condition)	Mole Fraction	0.0008901
Inlet pressure	MPa	7
Inlet temprature	K	310
Inlet velocity	m/s	315.36
Flow rate	MMSCMD	14.51

different ethanol vapor mass fractions. As condensation progresses, the air stream with higher ethanol vapor concentration tends to condense more ethanol which warms up the entire air stream due to the release of condensation latent heat. As ethanol vapor mass fractions increases, the Wilson point is more distinguishable.

Fig. 6 shows the simulation results for computed profiles of nucleation rate and condensed ethanol droplet radius across the diverging section of Laval nozzle for various ethanol vapor mass fractions at 3S entrance (throat). As shown in Fig. 6a, the nucleation process shifts towards throat as the ethanol vapor mass fraction increases, because super-saturation ratio becomes unity sooner for higher concentrations of ethanol vapors. It is also apparent that the nucleation process happens more fiercely for larger ethanol vapor mass fractions.

It is interesting to note that the first glance at Fig. 6a and b implies that droplet growth occurs even before the nucleation process starts. This is not true, because droplets growth should occur after the nucleation process. More detailed examination of the simulation results reveals that even at much earlier locations after the throat position, the nucleation process has been started but the corresponding values have much lower order of magnitudes as shown in the semi-log scale of Fig. 7. These values are not distinguishable in the linear scales of Fig. 6a. Fig. 6b shows that the droplet radius increases asymptotically until all the condensable vapor condenses. The initial kinks observed in all cases can be due to averaging procedure and may not be observed in practical situations.

3.2. Application of proposed model for various natural gas refining processes

It was clearly demonstrated in the previous section that the proposed model (which uses our new mass transfer approach) was able to efficiently and correctly predict the condensation rates

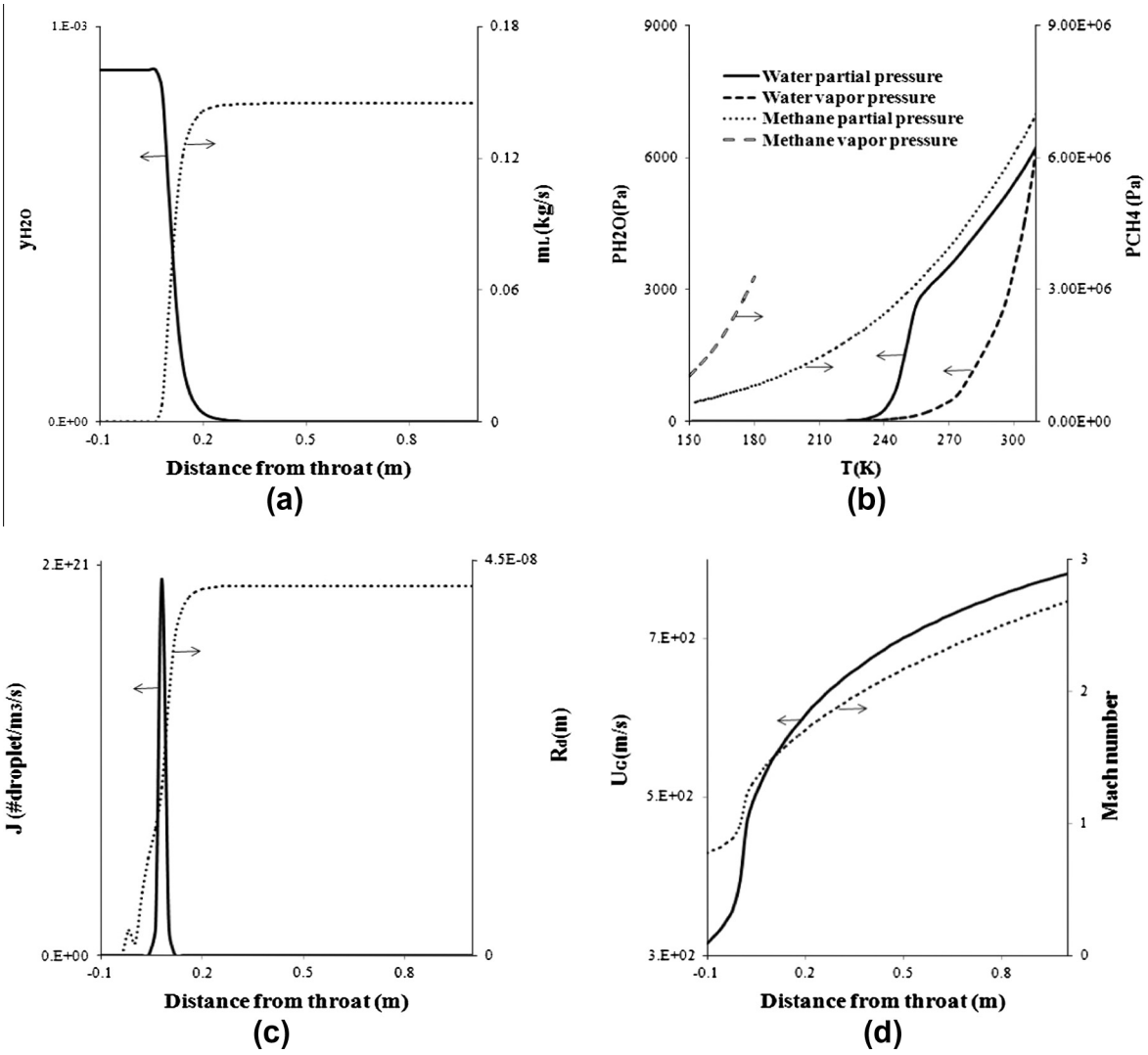

Fig. 8. Simulation results for the dehumidification of natural gas. (a) Water vapor mole fraction and cumulative liquid mass flow rate distributions (b) PT diagram for methane and water vapor (c) nucleation rate and mean droplet radius distributions and (d) gas velocity and mach number distributions.

during the travel of a mixture of ethanol and air through a 3S unit Laval nozzle. In this section, the same model will be employed to predict the behavior of similar systems on two important processes of dehumidification and sweetening which are essential for most natural gas industries. The results of three following case studies show the capability of 3S units on removal of water vapor and hydrogen sulfide from a methane rich natural gas.

3.3. Simulation of 3S unit for dehumidification of natural gas

Table 2 provides the nozzle geometries used for a typical natural gas dehumidification process. Table 3 presents the wet feed gas operating conditions and its corresponding analysis. The inlet velocity is selected via trial and error procedure to attain unit Mach number at throat location. Other operating conditions are used to mimic most of the dehumidification processes used in various natural gas industries.

Fig. 8 shows the simulation results for various distributions across the Laval nozzle of 3S unit. Fig. 8a clearly illustrates the powerful performance of the Laval nozzle on effective separation of water vapor from natural gas. As it can be seen in Fig 8b, the water vapor almost entirely condenses in the Laval nozzle while the methane rich gas remains as vapor. Note that the left and right sides of Fig. 8b belongs to the exit and inlet conditions, respectively. Fig. 8c and d illustrate the nucleation rate, mean droplet radius, gas velocity and corresponding Mach number distributions which support the obtained results presented in Fig. 8a and b. The minimum required Laval nozzle length can be selected when the amount of water vapor remaining in the natural gas at exit condition becomes less than the standard permissible value (7 lb_m/MMSCF).

3.4. Simulation of 3S unit for dry natural gas sweetening process

Tables 4 and 5 present the inlet sour gas operating conditions and its analysis for a typical natural gas sweetening process and the corresponding nozzle geometries. as mentioned earlier, the required overall Laval nozzle length is selected when the amount of hydrogen sulfide impurity remaining in the natural gas at exit condition becomes less than its standard permissible value (4 ppm).

As shown in Fig. 9a, the hydrogen sulfide impurity is entirely condenses and then separates (via the swirling effect of 3S unit which has not been considered here) from the rich methane natural gas. In is interesting to note in Fig. 9b that the hydrogen sulfide initially condenses after the throat location but before encountering Wilson point. At this stage (which can be realized by a small

Table 4
Nozzle parameters.

Parameter	Unit	Value
Inlet radius	m	0.0525
Inlet area	m^2	0.0087
Throat radius	m	0.05
Throat area	m^2	0.0079
Outlet radius	m	0.116
Outlet area	m^2	0.0423
Nozzle (converging) length	m	0.2
Diffuser (diverging) length	m	1.5

Table 5
Analysis and operating conditions of dry sour feed gas entering sweetening process.

Parameter	Unit	Value
CH_4 composition	Mole Fraction	0.95
H_2S composition	Mole Fraction	0.05
Inlet pressure	MPa	9
Inlet temprature	K	300
Inlet velocity	m/s	247.93
Flow rate	MMSCMD	15.89

kink in various curves of Fig. 9), the vaporization occur momentarily and then condensation proceeds until almost all of the hydrogen sulfide impurity condenses.

The Wilson point was not observable in Fig. 8 because the water vapor mole fraction was extremely small and its condensation cannot produce sufficient heat to establish Wilson point. As before, Fig. 9c and d illustrate the nucleation rate, mean droplet radius, gas velocity and corresponding Mach number distributions which support the obtained results presented in Fig. 9a and b.

3.5. Simulation of 3S unit for wet natural gas sweetening

In all real and practical natural gas sweetening processes, the sour feed gas is saturated with water vapor, because it leaves the three phase inlet separator prior to entering the sweetening process. For this reason, the assumption of dry sour gas is not valid in practice. Therefore, the proposed mass transfer approach is used in this section to predict the condensation rate when the natural gas is contaminated with both H_2S and water vapor. Evidently, the current binary approach may not be able to consider the interaction between the condensed water and liquid hydrogen sulfide during the condensation processes. Modeling the interactions of various liquids during multi-component condensation processes inside Laval nozzle is much challenging problem and will be dealt with later.

The nozzle geometries, natural gas composition and operating conditions are similar to those depicted in Tables 4 and 5, but the inlet sour gas stream is saturated with water vapor. Fig. 10 shows the simulation results for flow of wet natural gas across

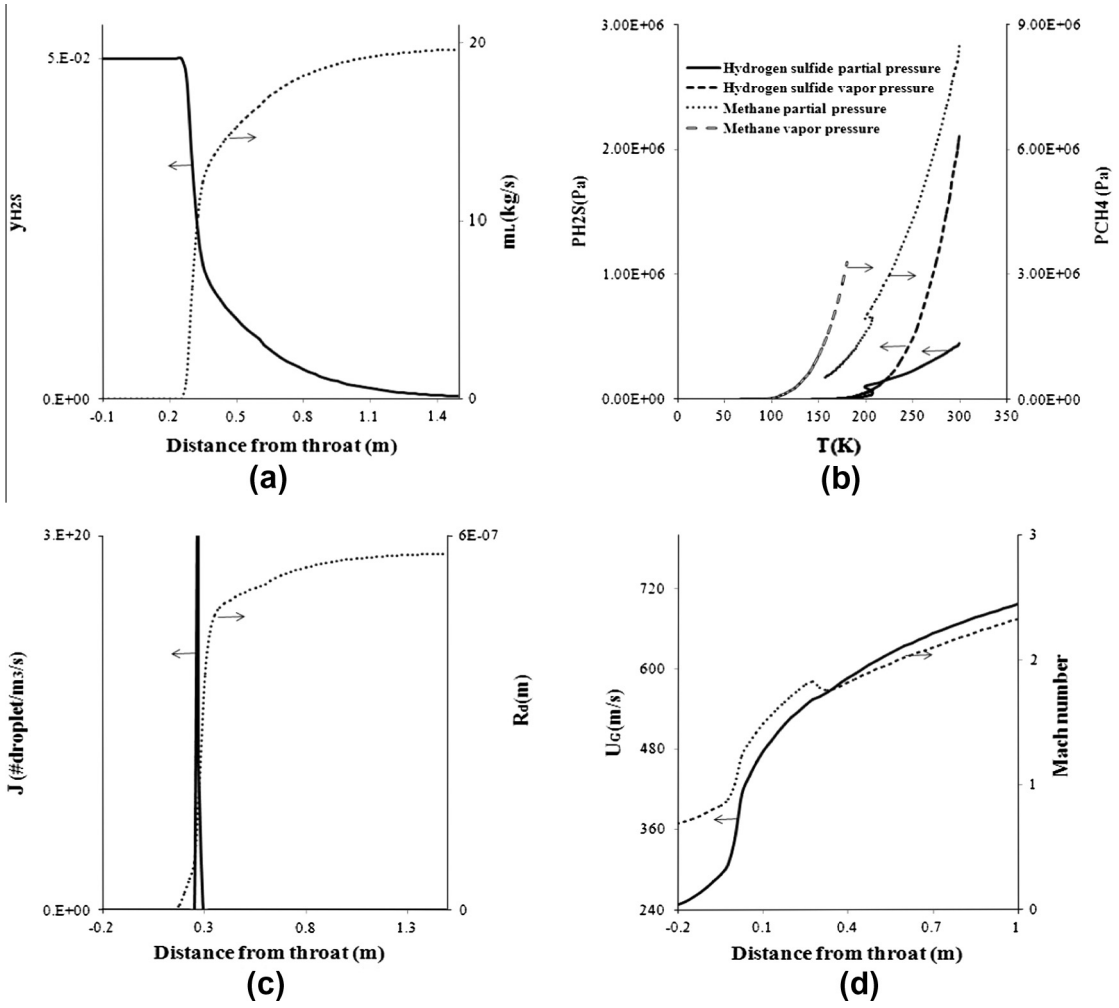

Fig. 9. Simulation results for sweetening case study: (a) water vapor mole fraction and cumulative liquid mass flow rate distribution, (b) PT diagram for methane and hydrogen sulfide, (c) nucleation rate and mean droplet radius distribution and (d) gas velocity and mach number distribution.

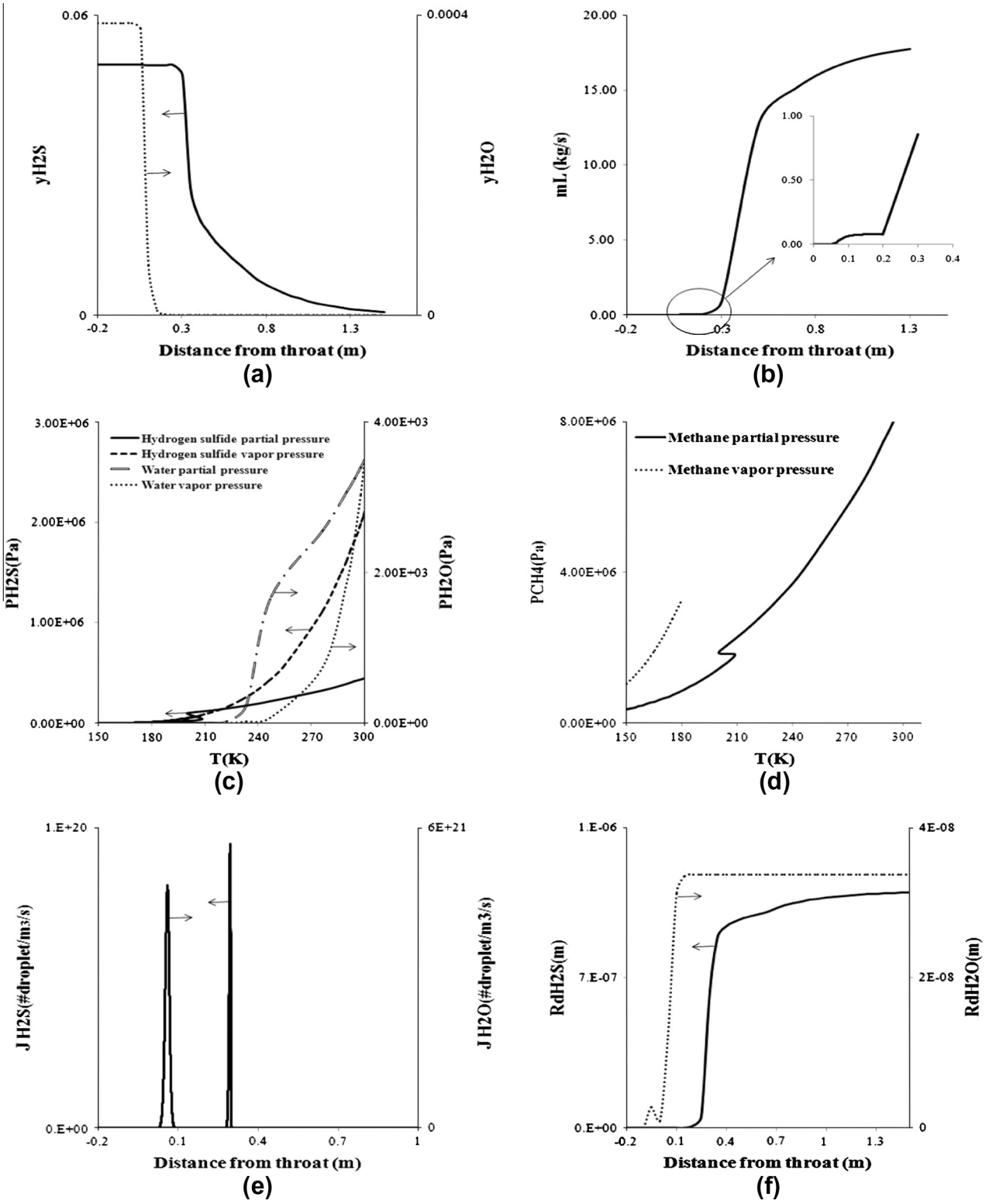

Fig. 10. Simulation results for wet natural gas sweetening case study:(a) Impurities mole fraction distribution (b) cumulative liquid mass flow rate distribution, (c) PT diagram for water vapor and hydrogen sulfide, (d) PT diagram for methane and (e) nucleation rate distribution for water vapor and hydrogen sulfide and (f) mean droplet radius distribution for water vapor and hydrogen sulfide.

the Laval nozzle of 3S unit employed for sweetening purpose. As shown in Fig. 10a, the 3S unit can efficiently separate both water vapor and hydrogen sulfide simultaneously from the wet sour natural gas stream.

It is interesting to note that in Fig. 10b the distribution of cumulative liquid mass flow rate has two distinguishable steps. The first one corresponds to condensation of water vapor while the second rise represents the condensation of hydrogen sulfide. Since the

amount of water vapor is much less than the hydrogen sulfide content of the sour wet gas, therefore, the first step is only can be identifies in the magnified version of Fig. 10b.

Fig. 10c shows that the condensation of water vapor occurs more readily than hydrogen sulfide. This is evident because the entering sour gas is saturated with water vapor. As illustrated in Fig. 10d, the methane phase envelop is far from its actual PT diagram inside Laval nozzle of 3S unit and therefore no condensation is anticipated. Fig. 10e and f shows that the nucleation process for water vapor occurs much earlier than hydrogen sulfide and the mean water droplet radius grows faster than hydrogen sulfide droplets. Both of these issues are in accordance with previous discussion.

4. Conclusion

Application of various gas–liquid separation devices is crucial in many chemical and petroleum engineering processes. Unlike other conventional gas–liquid separators, supersonic separators (3S) are able to receive a single phase feed stream and divide it into at least two separate phases. These advanced devices can dramatically increase the fluid velocity inside their Laval nozzle which leads to extra-cooled temperatures inside phase diagram of the condensable species.

Efficient prediction of temperature, pressure and composition profiles of various components during their travel inside Laval nozzle is vital for design and operation of 3S units. This task is not achievable until correct models are used for estimation of liquid droplet growth inside Laval nozzle. All previous works predicted the liquid droplet growth rate for pure component systems. A novel mass transfer approach is used here to develop a reliable model for estimation of liquid droplet growth rate for binary and multi-component systems. The model requires further improvements for multi-component systems where the interaction between condensed phases is appreciable.

The model predictions are initially validated very successfully for the experimental data of Wegener et al. for condensation of ethanol vapor from air stream. Then, the presented model is used to predict the performance of 3S unit for various natural gas processes, such as natural gas dehumidification and natural gas sweetening. It was clearly shown that the 3S unit can successfully achieve the permissible target values both water vapor and hydrogen sulfide content of natural gas while requiring a much more compact device compared to traditional processes used for dehumidification and sweetening purposes. Furthermore, the capital investments and the operating costs of the 3S unit are very lower than those traditional processes.

References

[1] S. Mokhatab, W.A. Poe, J.G. Speight. Handbook of natural gas transmission and processing, second ed., Burlington Gulf Professional Publishing, 2012.

[2] R. Faiz, M. Al-Marzouqi, Insights on natural gas purification: Simultaneous absorption of CO_2 and H_2S using membrane contactors, Sep. Purif. Technol. 76 (2011) 351–361.

[3] M.A. Aroon, A.F. Ismail, T. Matsuura, M.M. Montazer-Rahmati, Performance studies of mixed matrix membranes for gas separation: a review, Sep. Purif. Technol. 20 (2010) 229–242.

[4] I.A.A.C. Esteves, M.S.S. Lopes, P.M.C. Nunes, J.P.B. Mota, Adsorption of natural gas and biogas components on activated carbon, Sep. Purif. Technol. 62 (2008) 281–296.

[5] B.M. Vaziri, A. Shahsavand, H. Rashidi, M.G. Mazidi, Non isentropic performance of supersonic separators, in: 13th Iranian National Chemical Engineering Congress and 1st International Regional Chemical and Petroleum Engineering Kermanshah, Iran, 25–28 October, 2010.

[6] M. Ghanbari Mazidi, A. Shahsavand, B. M. Vaziri, Various pressure recovery scenarios for supersonic separators, J. Pet. Technol. (in press).

[7] F. Okimoto, J.M. Brouwer, Supersonic gas coditionning, World Oil Mag. 223 (2002) 89–91.

[8] H. Mohd, Z. Yusoff, N. Malek, Numerical modeling of wet steam flow in steam turbine channel, first ed., InTech, 2012.

[9] C. Wen, X. Cao, Y. Yang, J. Zhang, Supersonic swirling characteristics of natural gas in convergent-divergent nozzles, Pet. Sci. 8 (2011) 114–119.

[10] V.I. Alferov, L.A. Baguirov, L. Dmitriev, V. Feygin, S. Imaev, J.R. Lace, Supersonic nozzle efficiently separates natural gas components, Oil Gas J. 103 (2005) 53–58.

[11] M. Betting, H. Epsom, Supersonic separator gains market acceptance high velocities make a unique separator and dew pointer, World Oil Mag. 228 (2007) 197–200.

[12] P. Schinkelshoek, H. Epsom, Supersonic gas conditioning, GPA 87th Annual convention, Grapevine, TX, USA, March, 2008.

[13] V.I. Alferov, L.A. Baguirov, V. Feygin, A. Arbatov, S. Imaev, L. Dmitriev, V.I. Rezunenko, US Patent, 6372019, April 16, 2003.

[14] M. Betting, T. Van Holten, J. Van Veen. US Patent, 6524368, February 25, 2003.

[15] H. Liu, Z. Liu, Y. Feng, K. Gu, T. Yan, Characteristic of a supersonic swirling dehydration system of natural gas, Chin. J. Chem. Eng. 13 (2005) 9–12.

[16] E. Jassim, M.A. Abdi, Y. Muzychka, Computational fluid dynamics study for flow of natural gas through high-pressure supersonic nozzles: Part 1. Real gas effects and shockwave, Pet. Sci. Technol. 26 (2008) 1757–1772.

[17] E. Jassim, M.A. Abdi, Y. Muzychka, Computational fluid dynamics study for flow of natural gas through high-pressure supersonic nozzles: Part 2. Nozzle geometry and vorticity, Pet. Sci. Technol. 26 (2008) 1773–1785.

[18] M.M. Malyshkina, The structure of gas dynamic flow in a supersonic separator of natural gas, High Temp. 46 (2008) 69–76.

[19] A. Karimi, M.A. Abdi, Selective dehydration of high-pressure natural gas using supersonic nozzles, Chem. Eng. Process. 48 (2009) 560–568.

[20] M.M. Malyshkina, The procedure for investigation of the efficiency of purification of natural gas in a supersonic separator, High Temp. 48 (2010) 244–250.

[21] C. Wen, X. Cao, Y. Yang, Swirling flow of natural gas in supersonic separators, Chem. Eng. Process. 50 (2011) 644–649.

[22] C. Wen, X. Cao, Y. Yang, W. Li, Numerical simulation of natural gas in diffusers for supersonic separators, Energy 37 (2012) 195–200.

[23] C. Wen, X. Cao, Y. Yang, J. Zhang, Evaluation of natural gas dehydration in supersonic swirling separators applying the discrete particle method, Adv. Powder Technol. 23 (2012) 228–233.

[24] G. Gyarmath, On the growth rate of droplets in a supersaturated atmosphere, Z. Angew. Math. Phys 14 (1963) 280–293.

[25] J.B. Young, The spontaneous condensation of steam in supersonic nozzles, PhysicoChem. Hydrodyn. 3 (1982) 57–82.

[26] F. Bakhtar, K. Zidi, On the self diffusion of water vapor, Proc. Inst. Mech. Eng. Part C. 199 (1985) 159–164.

[27] G.Gyarmathy, Condensation in Flowing Steam. in: M.J. Moore, C.H. Sieverding (Ed.), Two-Phase Steam Flow in Turbines and Separators, Hemisphere, London, 1976.

[28] A. Koo, G.A. Brooks, M. Nagle, Nucleation and growth of Mg condensate during supersonic gas quenching, J. Cryst. Growth 310 (2008) 2659–2667.

[29] F. Bakhtart, M.T. Mohammadi Tochai, An investigation of two-dimensional flows of nucleating and wet steam by the time-marching method, Int. J. Heat Fluid Flow. 2 (1980) 5–18.

[30] A. Guha, J.B. Young, Time-marching prediction of unsteady condensation phenomena due to supercritical heat addition, I Mech. E Conf. Publ. (1991) 167–177.

[31] G. Cinar, B.S. Yilbas, M. Sunar, Study into nucleation of steam during expansion through a nozzle, Int. J. Multiphase Flow. 23 (1997) 1118–1171.

[32] A.J. White, M.J. Hounslow, Modeling droplet size distributions in polydispersed wet-steam flows, Int. J. Heat Mass Transfer. 43 (2000) 1873–1884.

[33] S. Dykas, Numerical calculation of the steam condensing flow, Task Q. 5 (2001) 519–535.

[34] A.G. Gerber, M.J. Kermani, A pressure based Eulerian–Eulerian multi-phase model for non-equilibrium condensation in transonic steam flow, Int. J. Heat Mass Transfer. 47 (2004) 2217–2231.

[35] M.R. Mahpeykar, A.R. Teymourtash, Effects of friction factor and inlet stagnation conditions on the self-condensation of steam in a supersonic nozzle, Sci. Iran Trans. B. 11 (2004) 269–282.

[36] Yong. Yang, Shengqiang. Shen, Numerical simulation on non-equilibrium spontaneous condensation in supersonic steam flow, Int. Commun. Heat Mass Transfer. 36 (2009) 902–907.

[37] S. Dykas, W. Wroblewski, Numerical modeling of steam condensing flow in low and high-pressure nozzles, Int. J. Heat Mass Transfer. 53 (2012) 933–945.

[38] S.H. Rajaee Shooshtari, A. Shahsavand, B. M. Vaziri, A theoretical mass transfer approach for prediction of droplets growth inside supersonic Laval nozzle, Unpublished results.

[39] M. Giordano, S.J. Hercus, P. Cinnella, Effects of modeling uncertainties in condensing wet-steam flows through supersonic nozzles, in: V European Conference on Computational Fluid Dynamics, Lisbon, Portugal, 14–17 June, 2010.

[40] J.E. McDonald, Homogeneous nucleation of water vapor condensation I. Thermodynamic aspects, Am. J. Phys 30 (1962) 870–877.

[41] J.B. Young, The condensation and evaporation of liquid droplets in a pure vapor at arbitrary knudsen number, Int. J. Heat Mass Transfer. 34 (1991) 1649–1661.

[42] G. Nagayama, T. Tsuruta, A general expression for the condensation coefficient based on transition state theory and molecular dynamics simulation, J. Chem. Phys. 118 (2003) 1392–1399.
[43] P. Wegener, A. Clumpner, B. Wu, Homogeneous nucleation and growth of ethanol drops in supersonic flow, Phys. Fluids 15 (1972) 1869–1876.
[44] R. Kumar, D.A. Levin, Simulation of homogeneous condensation of small polyatomic systems in high pressure supersonic nozzle flows using Bhatnagar-Gross-Krook model, J. Chem. Phys. 134 (2011).